J. Fluid Mech. (1988), *vol.* 188, *pp.* 529–546
Printed in Great Britain

Longitudinal vortices imbedded in turbulent boundary layers
Part 2. Vortex pair with 'common flow' upwards

By R. D. MEHTA
Department of Aeronautics and Astronautics, JIAA, Stanford University, Stanford, CA 94305, USA

AND P. BRADSHAW
Department of Aeronautics, Imperial College, London SW7 2BY, UK

(Received 10 July 1985 and in revised form 7 September 1987)

Detailed mean flow and turbulence measurements have been made in a low-speed turbulent boundary layer in zero pressure gradient with an isolated, artificially generated vortex pair imbedded in it. The vortices, generated by two half-delta wings on the floor of the wind-tunnel settling chamber, rotate in opposite directions such that the 'common flow' between the vortices is away from the surface, and the vortex pair draws boundary-layer fluid upwards. The distance of the vortex cores above the surface grows downstream, and is roughly twice the local boundary-layer thickness. The cancellation of circulation by mixing of fluid from the two vortices is slow, and the vortices are identifiable down the full length of the test section. As in the case of the single vortex investigated in Part 1 of this series, large changes in structural parameters of the turbulence occur.

1. Introduction

This paper is the second of a group dealing with longitudinal vortices imbedded in otherwise two-dimensional constant-pressure turbulent boundary layers. Part 1, by Shabaka, Mehta & Bradshaw (1985) dealt with a single vortex and Part 3, by A. D. Cutler & P. Bradshaw (in preparation), discusses a vortex pair with the 'common flow' between the vortices directed towards the surface, so that the vortices move apart laterally with a diverging boundary-layer flow between them. For an overview of these and related experiments see Bradshaw & Cutler (1987). Here we present measurements of the interaction between a boundary layer and a vortex pair with the 'common flow' upwards. Although the vortices are initially close to the solid surface, their cores rise to a height of roughly twice the thickness of the boundary layer, to which they are connected by a tongue of upward-moving fluid, with a corresponding lateral convergence of boundary-layer fluid towards the plane of symmetry. The conventional inviscid model of aircraft trailing vortices near the ground, composed of the two real vortices and their images under ground, at once shows that vortices with the common flow towards the surface stay close to the surface and move apart in the spanwise direction; but if in this inviscid model the vertical plane of symmetry, rather than the horizontal one, represents a solid surface, then the right-hand half (say) of the flow represents the present case of two vortices with common flow away from the surface, drawing closer together as they move away from the surface.

In Part 1 we outlined the importance of imbedded-vortex flows in general, and reviewed the rather small number of papers that throw direct light on the turbulence structure. Probably the most spectacular real-life case of a vortex pair with the common flow away from the surface is in the 'S-bend' intake used in the dorsal engines of several current civil jet aircraft and the side intakes of many military aircraft (Bansod & Bradshaw 1972; Taylor, Whitelaw & Yianneskis 1984). In this case, longitudinal vorticity is generated by lateral (circumferential) deflection of boundary-layer fluid by the pressure gradients in the first half of the 'S', leading to a vortex pair near the bottom surface of a dorsal intake: the vortex pair is then intensified by longitudinal acceleration and concave surface curvature in the second half of the bend, leading in turn to large circumferential non-uniformity of the flow at the engine face. A weaker vortex pair occurs on the convex surface of a single bend (Humphrey, Whitelaw & Yee 1981) where surface-curvature effects are stabilizing. A vortex pair with common flow upwards also appears, in principle, at the centreline of a wind-tunnel contraction wall, again because of lateral deflection of boundary-layer fluid (Mokhtari & Bradshaw 1983; Gessner, Ferguson & Lo 1986): fortunately, if the contraction ratio is large the boundary layer at exit is so thin that the vortex pair attenuates quickly.

In the present paper, we have retained the technique used in Part 1, in which vortices are generated by half-delta wings on the floor of the wind-tunnel settling chamber (followed by a 'two-dimensional' contraction with a reduction in height but not in width). The advantage of this configuration is that the circulation around a vortex is nominally conserved as it passes through a contraction, while percentage variations in axial velocity are greatly reduced, so that the vortex entering the working section is relatively pure and as close to the surface as possible. As in Part 1, the test-section boundary layer is at constant pressure and is nominally two-dimensional outside the vortex interaction region, so that changes in turbulence structure can be attributed directly to the vortex interaction rather than to complicating influences such as longitudinal pressure gradient. For a study of a configuration similar to that of Part 1, but including the effects of pressure gradient, see Westphal, Eaton & Pauley (1987); and for mean-flow measurements in a similar configuration to the present one see Pauley & Eaton (1987). Heat-transfer effects have been investigated by Eibeck & Eaton (1987).

Measurements were made with conventional hot-wire anemometers, the effect of inserting probes into these relatively weak vortices being negligible. The measurements include all three components of mean velocity, all six independent components of Reynolds stress, and all triple products, in each case at two or more streamwise stations. Here we present only a selection of results, mainly at 1350 mm from the start of the working section: full results are obtainable on digital magnetic tape from the authors. The object of the work was to contribute to the development and testing of engineering calculation methods for complex turbulent flows, with the expectation that only methods based directly on term-by-term modelling of the Reynolds-stress transport equations would have sufficient generality to be reliable in a range of vortex flows. This expectation seems to have been confirmed by the comparisons of Liandrat, Aupoix & Cousteix (1985) between a number of calculation methods, and the data of Part 1 and the present paper. The measurements allow evaluation of all the terms in the Reynolds-stress transport equations, with the exception of those involving the pressure fluctuations: spatial transport of Reynolds stress by pressure fluctuations appears to be fairly small compared with transport by triple products of velocity fluctuations, while 'scrambling' of the turbulence by the pressure–strain redistribution term provides the main sink in the shear-stress

transport equations and can be deduced fairly accurately by difference. We have not measured turbulent energy dissipation directly: the total dissipation can be deduced as the sum of all the other (measured) terms in the turbulent energy equation, and, since the Reynolds number is fairly high, an equal partition of dissipation can be assumed except near the solid surface.

As in Parts 1 and 3, the results demonstrate large changes in the dimensionless structure parameters of the turbulence (corresponding to the 'constants' in Reynolds-averaged turbulence models). The correlation coefficients for the different components of shear stress necessarily reverse sign within the interaction region, but take quite large numerical values of either sign: that is, the turbulence is strangely, but strongly, organized. Near the centreplane a 'tongue' of highly turbulent fluid is extruded away from the surface, so that contributions to the normal stresses and to the primary ($-\overline{uv}$) shear stress are large, but the shear correlation coefficient in the centreplane is only about -0.25 near the surface, compared with typical values of -0.5 in a two-dimensional boundary layer, and steadily decreases outwards. This seems to be an extreme example of the weakening of eddy organization by lateral convergence (see Patel & Baek 1987 for measurements on the lee side of a body of revolution at incidence). Triple-product behaviour is necessarily very complicated, and, for simplicity rather than to promote any particular turbulence model, we present the results as 'transport velocities'. A transport velocity is the ratio of a triple product to the Reynolds stress that it notionally transports: in the double-vortex flow, values of as much as 0.2 of the external-stream velocity are found, even in regions where the Reynolds stresses (the denominators of the definitions) are quite large – another example of strong organization. Turbulence modelling problems will not be discussed in detail, but we attempt to interpret the results in the context of term-by-term modelling of the Reynolds-stress transport equations.

2. Apparatus and techniques

The test rig and techniques were generally as in Part 1. The measurements were made in the floor boundary layer of a 762×127 mm (30×5 in.) open-circuit blower wind tunnel, at a speed of about 30 m s^{-1}. The boundary layer at entry to the working section was laminar and about 3 mm thick, and was tripped by a 1 mm diameter wire. The pair of half-delta-wing vortex generators had the same dimensions as the single generator used in Part 1 (semi-span 114 mm, leading-edge sweep 68°). The vortex generators were mounted close together on the floor of the wind-tunnel settling chamber, with the leading edges further apart than the trailing edges (angles of 'incidence' $\pm 12°$) to produce a trailing vortex pair with common flow upwards. The configuration was developed in the Department's 1.2×0.6 m (4×2 ft.) smoke tunnel, at approximately the same Reynolds number as the main tests. The circulation round each vortex at entry to the working section was about $2.23U_e$ mm: this is about 20% larger than for the single vortex in Part 1, probably because one half-delta acts as an image of the other, increasing the lift (strictly, side force) in the same way as 'ground effect'. As in Part 1, Pitot tubes and surface Pitot (Preston) tubes were used for auxiliary measurements, and, again as in Part 1, secondary-flow velocity and turbulence measurements were made with conventional constant-temperature cross-wire anemometry. Drift in calibration due to air-temperature variation was accounted for in the software. In the (y, z)-plane contour plots shown below, the vertical scale is exaggerated, by a factor of $\frac{5}{3}$ compared with the horizontal scale.

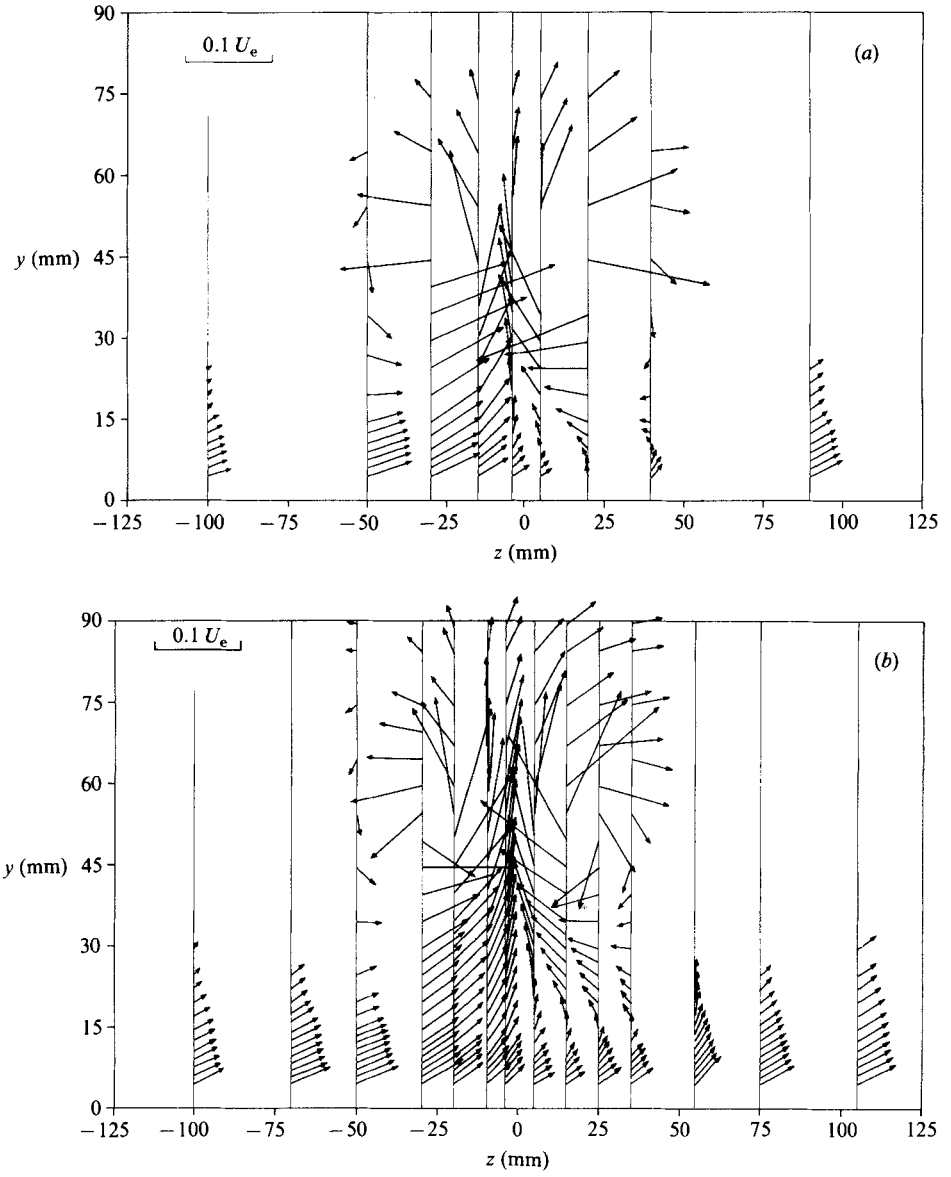

FIGURE 1. Secondary-velocity-vector plots (*a*) $x = 900$ mm: (*b*) 1350 mm.

3. Results

Although the flow in the region of the vortex cores themselves is acceptably symmetrical, the measurements show a crossflow angle of as much as 2° in the boundary layer beneath the vortices, superimposed on a symmetrical crossflow pattern induced by the vortices. Figure 1 shows quantitative results for the 'streamlines' in the secondary-flow (y, z)-plane, and figure 2 is a much-exaggerated qualitative sketch. The measurements were made in the same way as those of Part 1 and our other three-dimensional experiments, which showed no unexpected measured crossflow mean velocity W: also, the symmetry of the measurements in the

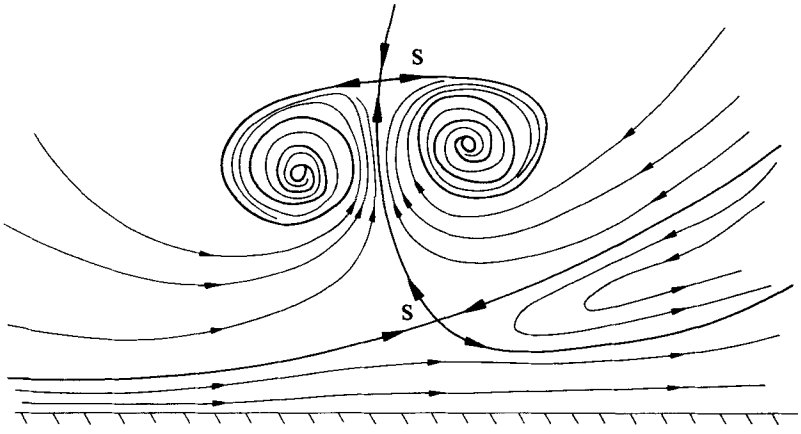

FIGURE 2. Schematic of 'streamlines' in crossflow (y, z)-plane: S = Saddle point: S–S is nominal line of symmetry.

vortex region suggests that there are no consistent errors W in that part of the flow. Near the wall, the mean-velocity gradient $\partial U/\partial y$ induces a spurious W in the reading of a cross-wire probe, but the spurious crossflow angle is roughly $0.05h/y$, where h is the distance between the two wires (typically 0.5 mm), and is thus no more than 0.005 rad ($\frac{1}{4}°$) at $y = 5$ mm. Therefore the asymmetrical W-pattern is likely to be real, rather than a consistent error: it appears in measurements at all x-positions and is certainly not a random error.

The measurements of Pauley & Eaton (1987), on a vortex pair with one vortex twice the strength of the other, showed very large asymmetry of crossflow even before the vortex core positions had become noticeably asymmetrical. This suggests that the crossflow in the present boundary layer may result from a rather small difference between the strengths of the two vortices.

The circulation implied by integrating $\partial W/\partial y$ over the region of the boundary layer shown in figure 1 is of the same order as the circulation in each vortex: however, this is almost completely cancelled by the opposite sign of $\partial W/\partial y$ closest to the surface, the difference being proportional to the (small) value of W at the boundary-layer edge. Also, of course, the boundary-layer circulation in the crossflow plane – insofar as it is real – must be a transfer from the z-wise vorticity in the boundary layer, $\partial U/\partial y$, by lateral skewing, rather than a loss from one of the vortices. Results presented below show that the plane of symmetry of the vortex pair is slightly displaced to one side of the tunnel centreplane, but the implied crossflow angle is only about 0.2°, of the same order as tunnel flow non-uniformities, and this near-symmetry suggests that the boundary-layer crossflow, however caused, does not greatly affect the flow in the vortex region.

Secondary flow velocities (figure 1) are as large as 0.1 of the axial velocity, and – correspondingly – the height of the interaction region is of the order of 0.05–0.1 of the streamwise distance x, several times the undisturbed boundary-layer thickness. The secondary velocities for the vortex pair are *more* than twice those obtained at a similar downstream distance for the single vortex in Part 1. Figure 3 shows the longitudinal vorticity contours obtained from differentiating the hot-wire measurements of figure 1: some of the smaller-scale variations, such as the asymmetrical cap of negative vorticity above the right-hand vortex, are probably finite-difference errors.

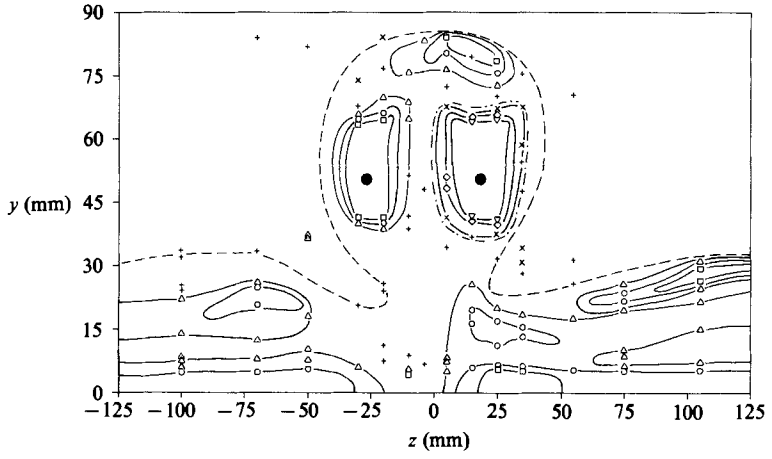

FIGURE 3. Contours of longitudinal vorticity $\xi/U_e = (\partial W/\partial y - \partial V/\partial z)/U_e$ mm^{-1}, $x = 1350$ mm. □, −0.0045; ○, −0.0030; △, −0.0015; +, 0; ×, 0.0015; ◇, 0.0030; ▽, 0.0045.

The maximum level of vorticity measured in the cores was about $0.018U_e$ mm^{-1}. The filled circles in figure 3 and later figures mark the positions of the vortex cores (maximum vorticity regions) as an aid to viewing. In the boundary layer the overall asymmetry noticeable in figure 1 naturally leads to asymmetry of the vorticity.

Figure 4 shows contours of the streamwise velocity, measured with a 1 mm diameter Pitot tube, at three stations. Static pressure variations were neglected in evaluating U, variations estimated from the secondary flow pattern being no more than 1% of the dynamic pressure. The velocity defect at the vortex-core position is no more than $0.01U_e$ at $x = 600$ mm. Flow-visualization tests confirmed that the main part of the vortex-generator wake was rolled up into the vortices, so the streamwise defect carried by the vortices is negligible. Naturally, the boundary-layer velocity contours are 'convected' by the secondary flow pattern into an outgoing wedge near the plane of symmetry, but the outermost contours at the first two stations are concave upwards, presumably as a result of the rather large displacement effect caused by the rapid growth of the vortex interaction region at small x, leading to high pressures on the plane of symmetry. Plots on semi-logarithmic axes (not shown here) are even more grossly distorted in the outer layer than in the case of the single vortex. As in Part 1, the friction velocity deduced from the reading of the 1 mm Pitot tube, placed on the wall and used as a Preston tube, collapses the near-wall profiles on the universal logarithmic law, both in slope and in intercept.

The low velocity near the surfaces at the centreplane, due to lateral convergence of boundary-layer fluid, naturally leads to low skin friction, as seen in figure 5. The sharpness of the variation suggests that lateral wandering of the vortex pair must be small. Wandering is also discussed by Westphal & Mehta (1987), who deliberately oscillated the vortex generator but found that its effects died out quite rapidly, in tacit agreement with the present results. The local maximum in skin friction near the centreline at $x = 600$ mm is not just a reading error, because it corresponds to the local minimum in distance of the axial velocity contours from the surface shown in figure 4(*a*); it is presumably part of the initial adjustment of the interaction near the point at which the vortices enter the boundary layer. However it may be 'configuration dependent', because Pauley & Eaton (1987) found no similar effect

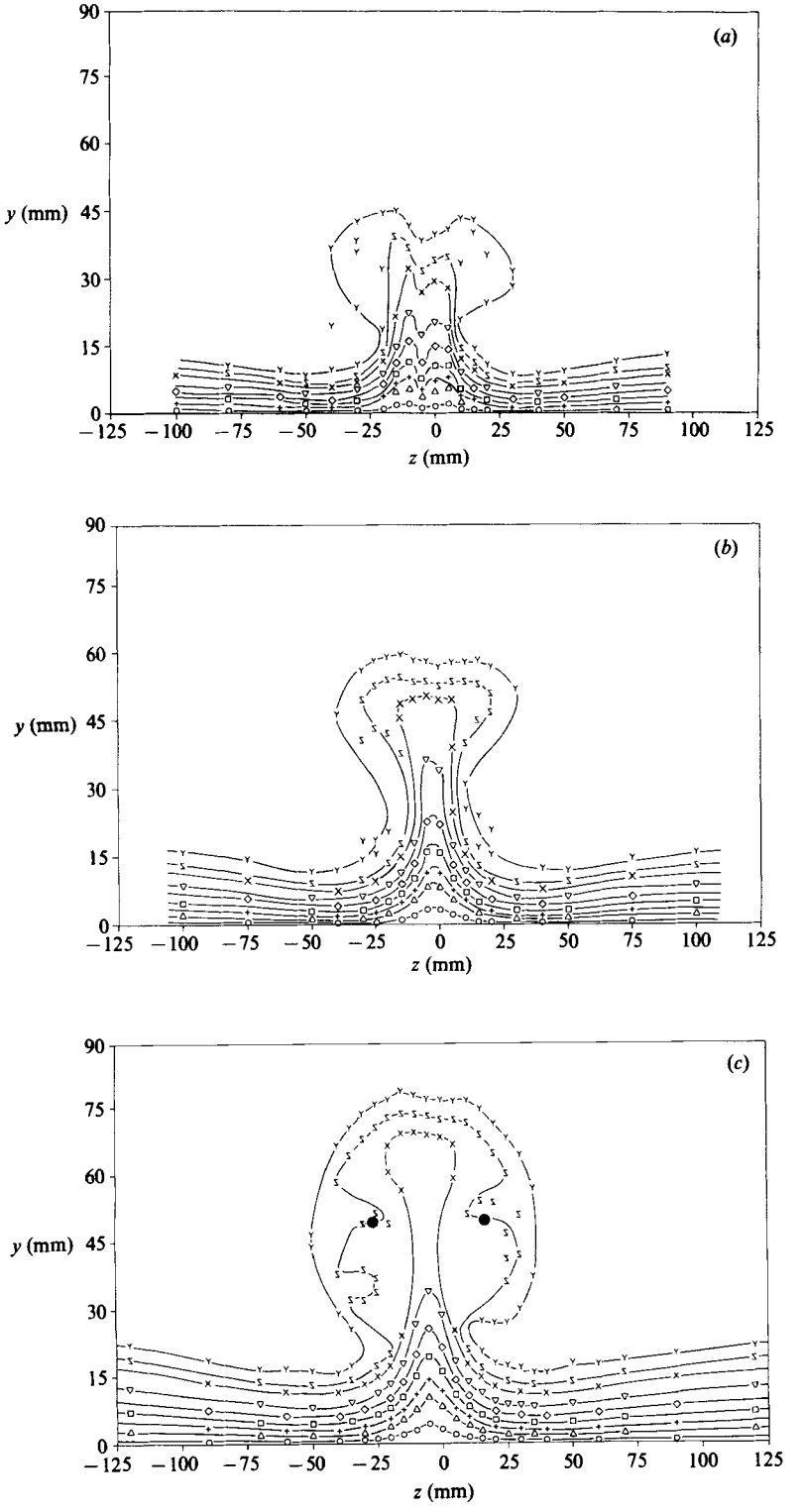

FIGURE 4. Contours of streamwise mean velocity. ○, $U/U_e = 0.6$; △, 0.7; +, 0.75; □, 0.8; ◇, 0.85; ▽, 0.9; ×, 0.95; Σ, 0.975; Y, 0.995. (*a*) x = 600 mm; (*b*) 900 mm; (*c*) 1350 mm.

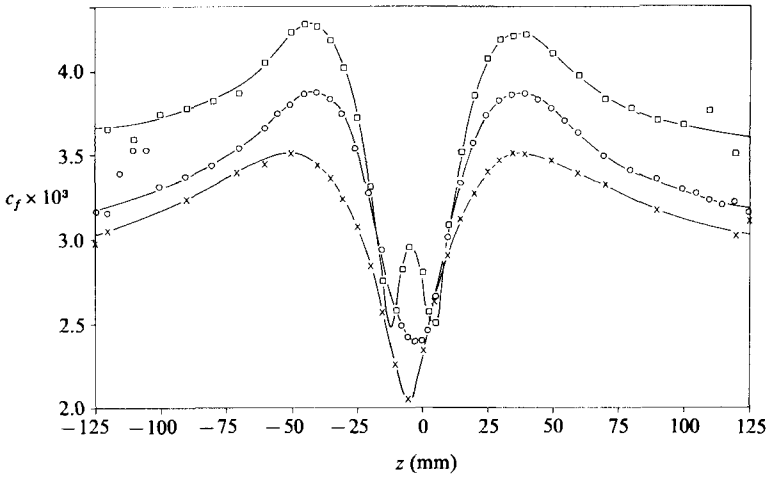

FIGURE 5. Spanwise variation of skin-friction coefficient $c_f = \tau_w/\frac{1}{2}\rho U_e^2$: □, $x = 600$ mm; ○, 900 mm; ×, 1350 mm.

although it is present in the measurements of Eibeck & Eaton (1987). The peaks in skin friction at either side of the centreline are not trivial to explain. As seen in figure 4, negative V tends to thin the boundary layer, and outweighs the thickening due to lateral convergence, but it is certainly not obvious that net maxima of c_f, too large to attribute to Reynolds-number effects alone, should occur. In Part 3, we show that minima of skin friction occur outboard of a vortex pair with 'common flow' downwards, with maxima inboard of the vortices but again with a mild minimum on the centreline.

Figures 6 and 7 show contours of all six independent Reynolds stresses, at $x = 1350$ mm only: results for $x = 900$ mm (all results are available in machine-readable form from the authors) are very similar. The longitudinal-component turbulence in figure 6(*a*) is qualitatively what would be expected from convection of pre-existing boundary-layer turbulence by the vortices. The wavy contours near the vortex cores result from the near-constant turbulence intensity in these regions and should not be taken too seriously. Figures 6(*b*) and 6(*c*) show spectacular (and closely symmetrical) maxima of vertical and lateral-component turbulence intensity in the vortex-core regions. This is further evidence that there is no large-scale lateral wandering of the vortices, which would almost certainly lead to large u-component fluctuations in regions of large $\partial U/\partial z$, and would also smear out the peaks in v- and w-component intensity. The differences in figures 6(*b*) and 6(*c*) are interesting in themselves, particularly near the centreplane, where $\overline{w^2}$ has a rather pronounced maximum near $y = 40$ mm while $\overline{v^2}$ does not.

Figure 7 shows the Reynolds shear stresses: the somewhat asymmetrical contours of $\overline{uv}$ in figure 7(*a*) may be partly attributable to inadequate spanwise resolution. We note the significant regions of positive $\overline{uv}$ (negative shear stress) above and outboard of the vortex cores, and the 'cap' of negative $\overline{uv}$ above the vortex pair. As in Part 1, we use separate dotted lines for '0−' and '0+' contours, intended to enclose negative and positive regions respectively: the concept of 'enclosure' is not rigorous. The contours in figures 7(*b*) and 7(*c*) are expected to be antisymmetrical about the centreplane $z = 0$: this is generally the case in the vortex region. The departure from antisymmetry nearer the surface is in the sense expected from the flow of boundary-

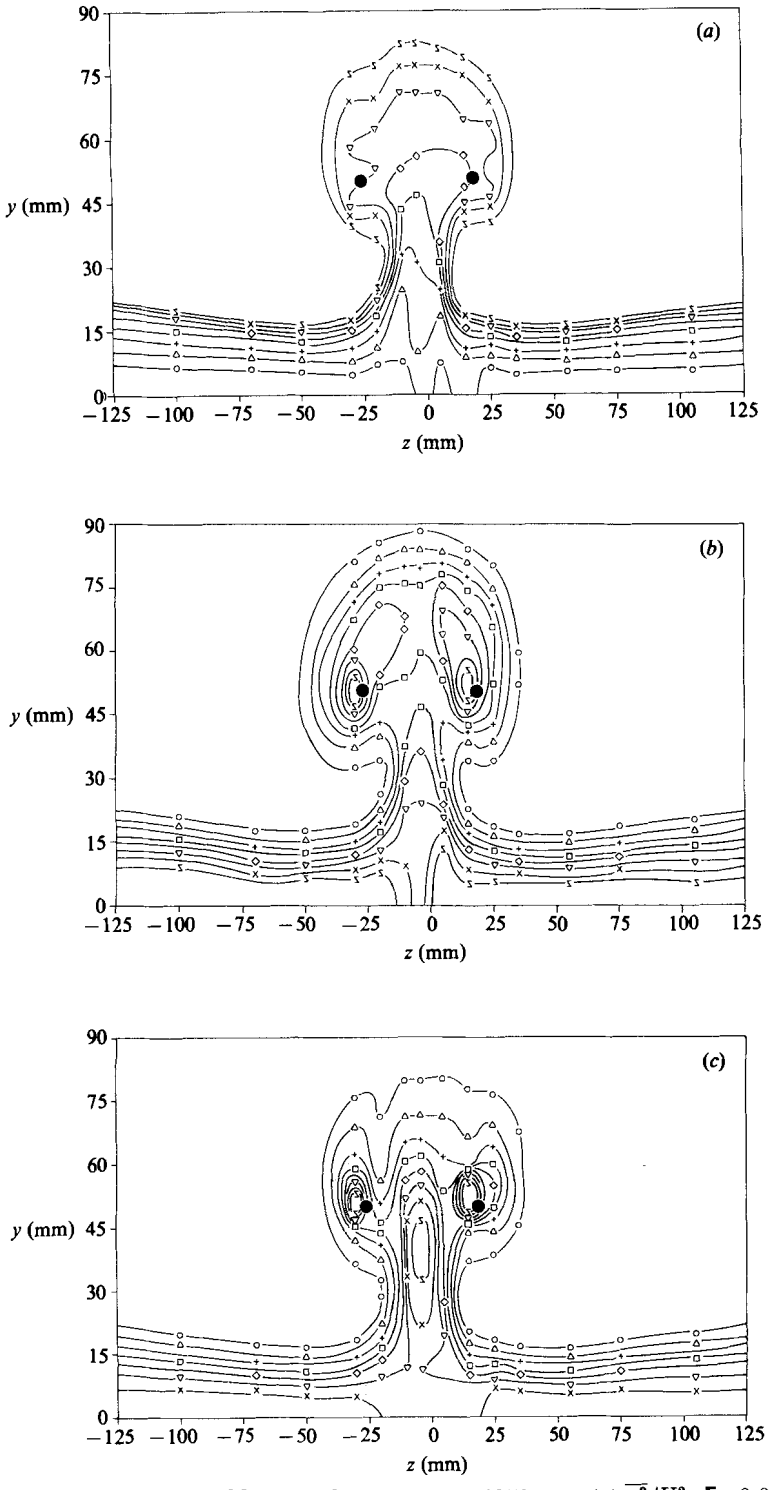

FIGURE 6. Contours of Reynolds normal stresses, $x = 1350$ mm. (*a*) $\overline{u^2}/U_e^2$: Σ, 0.0005; ×, 0.00075, ▽, 0.001; ◇, 0.0015; □, 0.002; +, 0.003; △, 0.004; ○, 0.005. (*b*) $\overline{v^2}/U_e^2$: ⊙, 0.0002; △, 0.0004; +, 0.0006; □, 0.0008; ◇, 0.0010; ▽, 0.0012; ×, 0.0014; Σ, 0.0016. (*c*) $\overline{w^2}/U_e^2$: ○, 0.0003; △, 0.0006; +, 0.0009; □, 0.0012; ◇, 0.0015; ▽, 0.0018; ×, 0.0021; Σ, 0.0024.

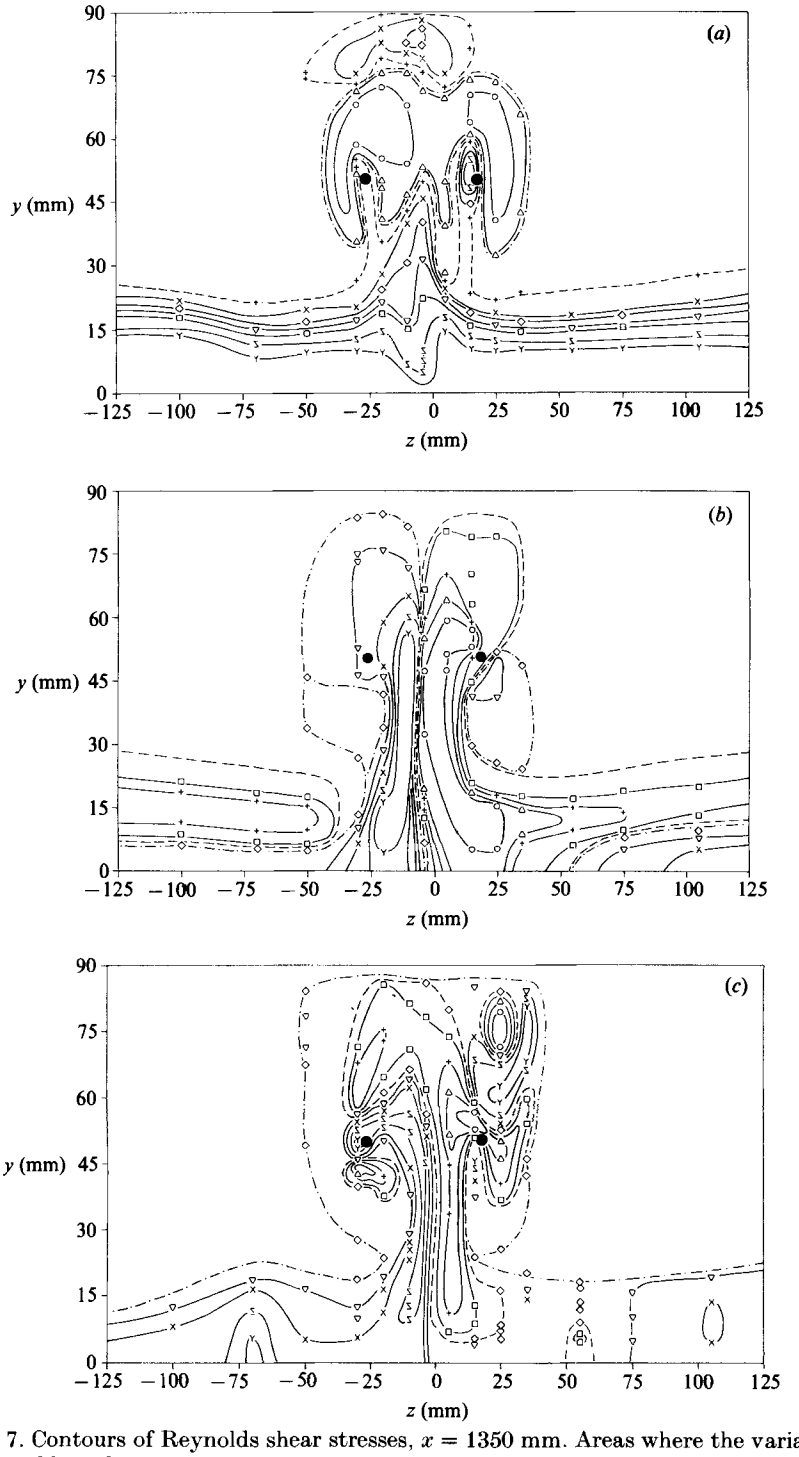

FIGURE 7. Contours of Reynolds shear stresses, $x = 1350$ mm. Areas where the variable is positive are enclosed by a dash-dot line, negative areas by a dashed line. (*a*) $\overline{uv}/U_e^2$: ○, 0.00015; △, 0.00005; +, 0.0; □, −0.00005; ◇, −0.0001; ▽, −0.0002; ×, −0.0003; ⅀, −0.0005; Y, −0.0007. (*b*) $\overline{uw}/U_e^2$: ○, −0.0004; △, −0.0003; +, −0.0002; □, −0.0001; ◇, 0.0; ▽, 0.0001; ×, 0.0002; ⅀, 0.0003; Y, 0.0004. (*c*) $\overline{vw}/U_e^2$: ○, −0.0004; △, −0.0002; +, −0.0001; □, −0.00005; ◇, 0.0; ▽, 0.00005; ×, 0.0001; ⅀, 0.0002; Y, 0.0004.

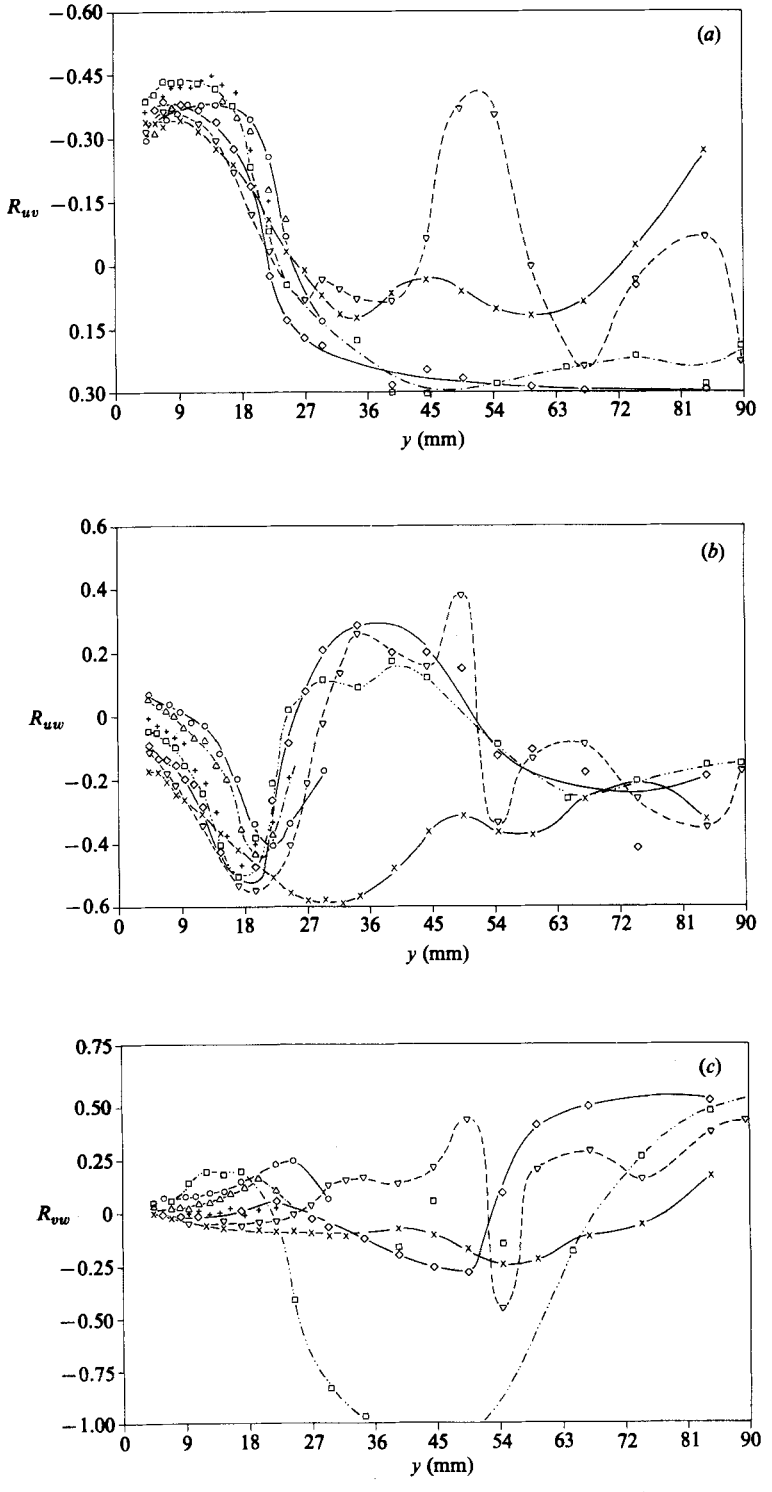

FIGURE 8. Profiles of shear correlation coefficients, $R_{uv} = -\overline{uv}/(\overline{u^2}\overline{v^2})^{\frac{1}{2}}$, R_{uw} and R_{vw}, $x = 1350$ mm. —○—, $z = 105$ mm; △, 75; □-·-□, 35; -◇-, 25; --▽--, 15; ×--×, 5. (*a*) R_{uv}, $z > 0$; (*b*) R_{uw}, $z > 0$; (*c*) R_{vw}, $z > 0$.

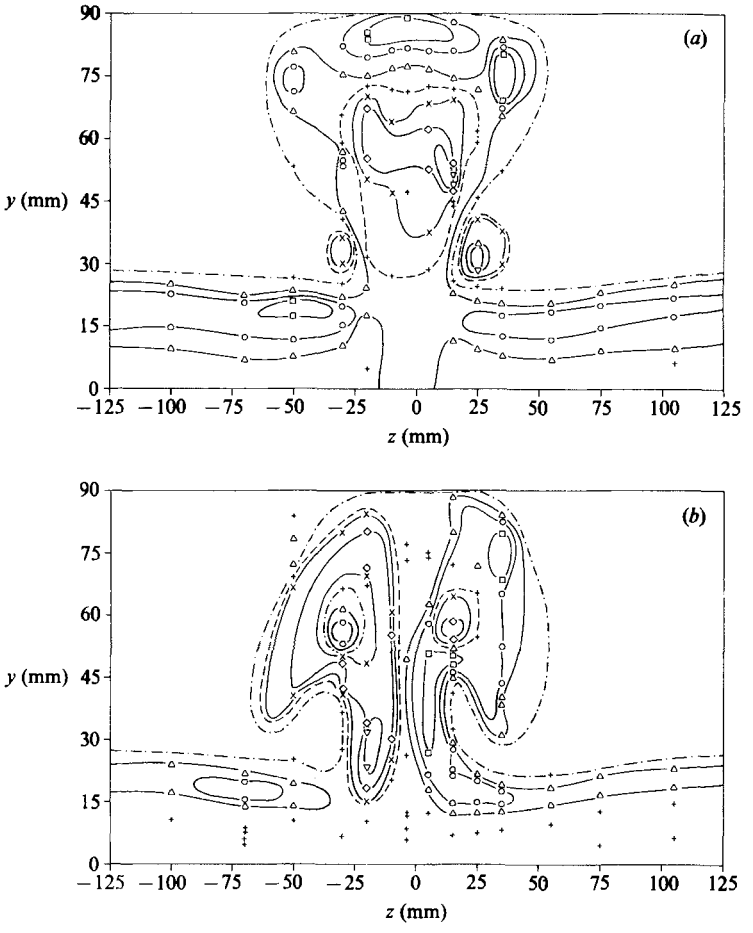

FIGURE 9. Transport velocities of turbulent kinetic energy, $x = 1350$ mm. (*a*) $V_q/U_e = \overline{q^2v}/(q^2U_e)$: □, 0.015; ○, 0.010; △, 0.005; +, 0; ×, −0.005; ◇, −0.010; ▽, −0.015. (*b*) $W_q/U_e = \overline{q^2w}/(q^2U_e)$: □, 0.020; ○, 0.010; △, 0.005; +, 0; ×, −0.005.

layer fluid from left to right seen in the secondary-velocity plots (figure 2). The qualitative explanation for the behaviour of the three Reynolds shear stresses is that each *tends* to transport momentum from high-velocity to low-velocity regions, and that the vortices tend to rotate fluid about the x-axis. For example, near the right-hand, clockwise-rotating, vortex, initially negative $\overline{uv}$ rotates to give negative $\overline{uw}$; and initially negative $\overline{uw}$, generated in the region of positive $\partial U/\partial z$ in the upswept fluid, can be convected and rotated round the vortex to give positive $\overline{uv}$ above and to the right of the vortex. Recall from figure 3 that the longitudinal mean vorticity exceeds $0.003U_e$ mm^{-1} over a large part of the vortex core at $x = 1350$ mm, implying that the rate of rotation is locally about one-quarter revolution per metre of streamwise travel, with much higher values further upstream: thus, rotation through angles of the order of 90° certainly occurs. Passive rotation of the stress tensor appears explicitly in the Reynolds-stress transport equations – for instance, the $\overline{uw}$ transport equation contains a term $-\overline{uv}\,\partial W/\partial y$ – but may be expected to influence the other terms as well, and thus affect the constants in a turbulence model.

Figure 8 shows a small selection of y-profiles for the correlation coefficients of the three components of shear stress, R_{uv}, R_{uw} and R_{vw}: they are intended merely to show the (large) typical values away from the zero crossings. R_{uv} is about -0.40 to -0.45 in the boundary layer at large z, but near the centreplane (e.g. $z = 5$ mm) the values are smaller even within the boundary layer, and R_{uv} takes positive values (transport of high-momentum fluid away from the surface) immediately underneath the vortex cores. We see that dimensionless turbulence parameters, as well as the Reynolds stresses, are grossly disturbed, even more than in the single-vortex flow. However, the large numerical values of all three coefficients imply that the vortices modify, but certainly do not destroy, the anisotropy of the turbulence.

Figure 9 shows the v- and w-component transport velocities of turbulent energy, defined as

$$V_q = \frac{\overline{u^2v} + \overline{v^3} + \overline{w^2v}}{\overline{u^2} + \overline{v^2} + \overline{w^2}}, \quad W_q = \frac{\overline{u^2w} + \overline{v^2w} + \overline{w^3}}{\overline{u^2} + \overline{v^2} + \overline{w^2}}.$$

Strictly both definitions should include pressure-fluctuation terms, but these are not currently measurable: the pressure contribution to V_q is small near the outer edge of a plane boundary layer – about the only place where it can be checked by difference – but this is very slender evidence for smallness of pressure contributions to V_q and W_q throughout the present flow. V_q should obviously be symmetrical, and W_q antisymmetrical, about the centreplane: the positions, if not the values, of the extrema are indeed symmetrical. As usual, the general tendency is for turbulent energy to be transported from high-energy regions (specifically, the vortex cores) to the lower-intensity regions around them. In addition, there is a region of large upward transport velocity at the top of the interaction region, which might be expected, but there is also a significant region of *downward* transport in between the vortex cores, in a region where $\overline{w^2}$, at least, is decreasing fairly strongly with increasing y – that is, this is a region of counter-gradient transport. W_q, shown in figure 9(*b*), has pronounced extrema close to the vortex-core positions: these are regions of maximum turbulent energy, so that gradient-diffusion concepts would imply negligible triple-product transport in those regions.

Figure 10 shows one of the transport velocities for Reynolds shear stress, the V-component transport velocity of $\overline{uv}$ defined as

$$V_{uv} = \frac{\overline{uv^2}}{\overline{uv}}.$$

Maximum values are very much larger than for the transport velocities of turbulent energy, and it is difficult to believe that the same physical processes are responsible for both. In particular, V_{uv} in the vortex-core region is as large as 0.2 times the free-stream velocity. V_{uv} is generally positive (both numerator and denominator being negative) but negative values occur in the top 'cap', where $\overline{uv}$ is positive, and in and below the cores where $\overline{uv^2}$ is positive. Positive $\overline{uv^2}$ is also found close to the surface, but the corresponding transport velocities are too small to show up in the contour plots.

Figure 11 shows sample profiles of eddy diffusivities of momentum ('eddy viscosity', for $\overline{uv}$ only) and of Reynolds stresses (for $\overline{uv^2}$ only), normalized in the conventional fashion with the external-stream velocity and the *undisturbed* displacement thickness. Note that the normalized eddy viscosity in the outer layer of a plane boundary layer is about 0.017. Full contour plots have not been derived: it is clear that the eddy viscosities are highly eccentric and unlikely to be represented by simple algebraic formulae or even by transport equations.

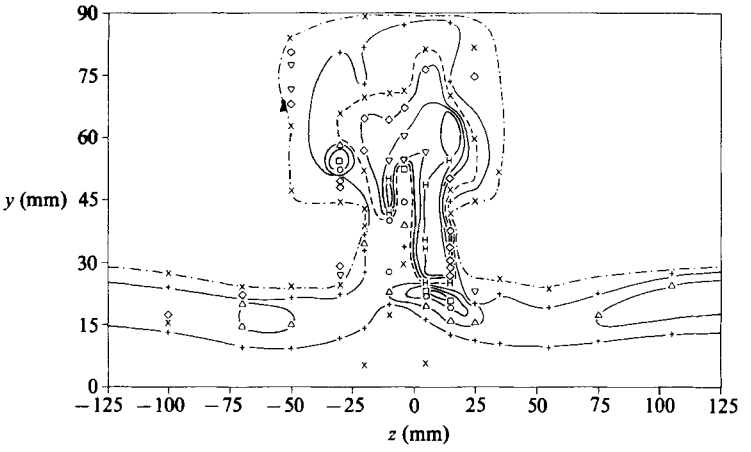

FIGURE 10. V-component transport velocity of turbulent shear stress, $V_{uv}/U_e = \overline{uv^2}/(\overline{uv}U_e)$: $x = 1350$ mm. □, 0.20; ○, 0.10; △, 0.05; +, 0.025; ×, 0.0; ◇, −0.025; ▽, −0.05; H, −0.10.

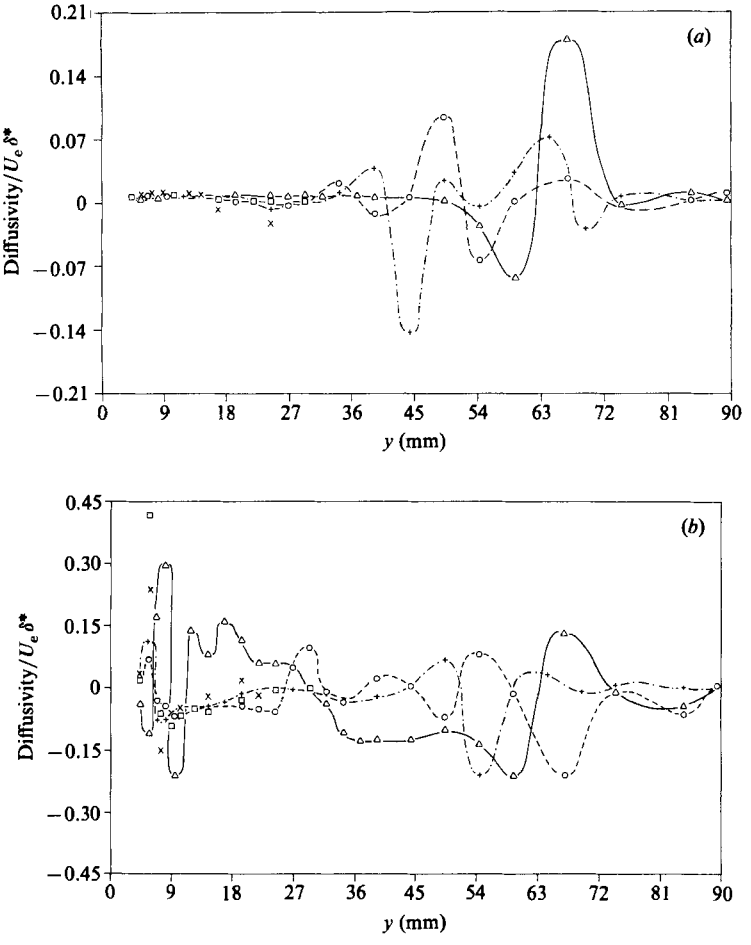

FIGURE 11. Profiles of eddy diffusivities, $x = 1350$ mm, normalized by $U_e\delta^*$, where δ^* is the undisturbed displacement thickness. (*a*) $-\overline{uv}/(\partial U/\partial y)$: □, $z = 105$ mm; --○--, 15; -△-, −3.75; +-·-+, −30; ×, −100. (*b*) $\overline{uv^2}/(\partial\overline{uv}/\partial y)$, symbols as in (*a*).

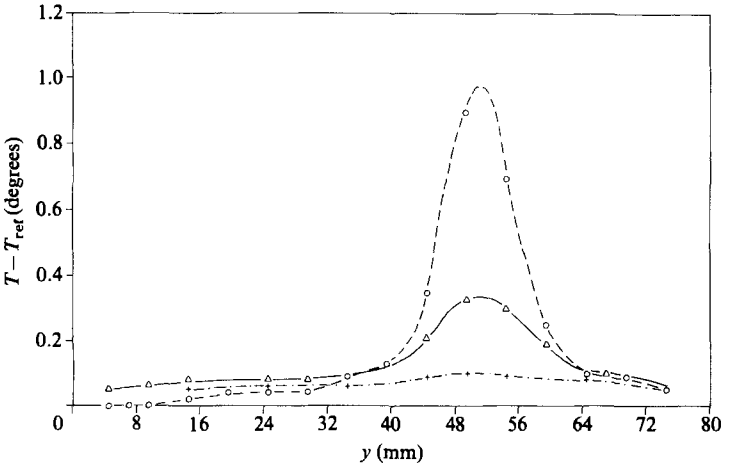

FIGURE 12. Mean temperature profiles, with upstream heat addition to negative-z vortex. –○–, $z = -30$ mm; --△--, -20; -+-, -10.

Figure 12 shows temperature profiles, resulting from heating one vortex as it left the vortex generator, as described in Part 1. The profile at $z = -30$ mm passes through the vortex core and gives an indication of the maximum temperature: the other two profiles, between the vortex core and the centreplane, show very much smaller temperature changes, demonstrating that scalar diffusion from one vortex into the other is small. This reinforces the picture of small diffusion of momentum and vorticity given by, for example, figure 3.

4. Discussion

The Reynolds-stress transport equations, and turbulence models based on them, contain minor explicit terms representing distortion and rotation by the mean flow. In the present case, as in Part 1 and in other complex-flow experiments, these terms represent experimental results only qualitatively, at best. The implication is that the major (generation or destruction) terms in the transport equations are quantitatively affected by distortion: their exact mathematical forms are still valid, but empirical models must be modified. As a general principle, 'constants' (empirical coefficients) in turbulence models are, or as of right ought to be, closely related to dimensionless structure parameters, and the latter will change if the structure is strongly perturbed. That is, even at local-equilibrium level, the simplest acceptable model must be of the form

$$\begin{aligned}\text{'empirical coefficient'} &= f\,(\text{structure parameter})\\ &= F\,(\text{dimensionless distortion rate})\\ &= F\,([\text{distortion rate}]/(\partial U/\partial y]).\end{aligned}$$

In the vortex regions in the present flow, the structural modifications – e.g. changes in shear correlation coefficients – are evidently rather large.

The boundary layer underneath the vortices suffers strong lateral convergence (i.e. negative $\partial W/\partial z$), but, as in the single vortex flow, apparently universal logarithmic regions can always be distinguished in the mean-velocity profiles close to the surface, where the ratio of mean shear $\partial U/\partial y$ to lateral convergence $-\partial W/\partial z$ is necessarily large. The relatively small circulation of the vortices in the present experiments leads

to crossflow angles of no more than about 5°, less than occur in many swept-wing boundary layers, and therefore we do not expect gross perturbations to the boundary layer as such. However, lateral convergence significantly reduces the Reynolds-stress correlation coefficient in the centreplane. A low surface shear stress near the centreplane is expected, because of the accumulation of low-velocity fluid, but it is not obvious that maxima of skin-friction coefficient should necessarily occur outboard of the vortices.

At a higher level of discussion, transport-equation modelling requires empirical correlations for the triple-product transport terms, and our results show quite complicated behaviour even of the 'bulk-transport' velocity, in which a given triple product is divided by the Reynolds stress that it transports. In particular, transport velocities for different Reynolds stresses are different by up to an order of magnitude, seriously undermining the *concept* of 'bulk transport' at some representative large-eddy eruption velocity. The alternative model for turbulent transport, eddy diffusivity, is taken over from the kinetic theory of gases with small mean free paths, and must be expected to fail in such a highly inhomogeneous flow. As in Part 1, the eddy diffusivities of Reynolds stress, to say nothing of the eddy viscosities, behave in a way that would be virtually impossible to correlate empirically.

Unfortunately, there do not seem to be useful quantitative correspondences between the present type of vortex pair and the spanwise-infinite array of Taylor–Görtler vortices found on concave surfaces (e.g. Hoffman, Muck & Bradshaw 1985). Crudely speaking, a given concave-surface vortex is a member of one pair with the common flow upwards, as in the present paper, and of another pair with the common flow downwards, as in Part 3 of the present series. It may be doubted whether any description of turbulence less complicated than the full Navier–Stokes equations can be expected to deal both with skew-induced vortices of the present sort *and* with curvature-induced vortices, so that empirical constants in Reynolds-averaged turbulence models would have to be chosen separately for each case. So far, there seem to have been no large-eddy or direct simulations of skew-induced vortices, and the direct simulation of curved-channel flow by Moser & Moin (1987) relies on spanwise periodicity to simplify the boundary conditions. However, large-eddy simulations include calculations of pressure fluctuations, which are currently unmeasurable, and a combination of experiment and simulation is probably essential for the development of reliable Reynolds-averaged turbulence models for imbedded vortex flows.

One of the few attempts to predict imbedded-vortex flows with present-day turbulence models is that of Liandrat *et al.* (1985), who used mixing-length, k–ϵ and stress-transport models on the data of Part 1 and the present paper. For the single vortex of Part 1, the predictions of the spanwise-plane shear stress $-\overline{uw}$ are scarcely recognizable, even in the case of the Reynolds-stress model. In the case of the double vortex investigated in the present work, the predicted vortex regions are much too tall and slender: the measured ratio of vortex-region height to width, at the contour $U/U_e = 0.995$, is about 1.57 whereas both the mixing-length and k–ϵ models predict ratios over 2. That is, a competent application of existing models to the present results produces results that are not adequate for engineers.

5. Conclusions

Detailed measurements of the interaction between a vortex pair (with the 'common flow' away from the surface) and a two-dimensional boundary layer show

a more complex picture than in the case of a single imbedded vortex. Boundary-layer fluid is lifted up by the vortices, and entrained into them, but there is very little direct interaction between the vortices. Strong, concentrated maxima of lateral- and vertical-component intensity occur in the vortex cores, but there is no sign of large-scale wandering of the vortices – which, like most kinds of low-frequency unsteadiness, would greatly complicate turbulence modelling. There are significant effects of lateral convergence in the boundary layer before it is swept up into the vortices: for example, the shear-stress correlation coefficient is considerably smaller near the plane of symmetry than in the undisturbed boundary layer. In the vortex region, large changes occur in all the dimensionless structural parameters of the turbulence. As in the case of the single imbedded vortex, eddy viscosities and diffusivities are *very* ill behaved, to the extent that contours are not plottable. In the single-vortex flow, apparent 'bulk transport' velocities of the Reynolds stresses were better behaved than eddy diffusivities, but in the present flow these too are ill behaved, as well as too large to be plausible velocities of fluid in the eddies. This suggests that the whole concept of large eddies that control transport may be inapplicable in highly complex flows. Prediction of imbedded-vortex flows will require a full Reynolds-stress-transport model flow (i.e. term-by-term modelling of the transport equation), but comparisons by Liandrat *et al.* (1985) between the present data sets and several prediction methods suggests that even the best current Reynolds-averaged models are inadequate. Complex flows like the present one are beyond the reach of current time-dependent Navier–Stokes simulation programs (Rogallo & Moin 1984) so that, in the study of complex turbulent flows, computers will not replace wind tunnels in the near future.

REFERENCES

Bansod, P. & Bradshaw, P. 1972 The flow in S-shaped ducts. *Aero. Q.* **23**, 131.

Bradshaw, P. & Cutler, A. D. 1987 Three-dimensional flows with imbedded longitudinal vortices. In *Perspectives in Turbulent Studies* (ed. H. U. Meier & P. Bradshaw), p. 382. Springer.

Eibeck, P. A. & Eaton, J. K. 1987 Heat transfer effects of a longitudinal vortex embedded in a turbulent boundary layer. *Trans. ASME* C: *J. Heat Transfer* **109**, 16.

Gessner, F. B., Ferguson, S. D. & Lo, C. H. 1986 Experiments on supersonic turbulent flow development in a square duct. *AIAA*-86-1038.

Hoffmann, P. H., Muck, K. C. & Bradshaw, P. 1985 The effect of concave surface curvature on turbulent boundary layers. *J. Fluid Mech.* **161**, 371.

Humphrey, J. A. C., Whitelaw, J. H. & Yee, G. 1981 Turbulent flow in a square duct with strong curvature. *J. Fluid Mech.* **103**, 443.

Liandrat, J., Aupoix, B. & Cousteix, J. 1987 Calculation of longitudinal vortices imbedded in a turbulent boundary layer. In *Turbulent Shear Flows 5* (ed. F. Durst *et al.*), p. 253. Springer.

Mokhtari, S. & Bradshaw, P. 1983 Longitudinal vortices in wind tunnel wall boundary layers. *Aero J.* **87**, 233.

Morton, B. R. 1984 The generation and decay of vorticity. *Geophys. Astrophys. Fluid Dyn.* **28**, 277.

Moser, R. D. & Moin, P. 1987 The effects of curvature in wall-bounded turbulent flows. *J. Fluid Mech.* **175**, 479.

Patel, V. C. & Baek, J. H. 1987 Boundary layers in planes of symmetry. Part 1. Experiments in turbulent flow. *AIAA J.* **25**, 550.

Pauley, W. C. & Eaton, J. K. 1987 An experimental study of the development of longitudinal vortex pairs embedded in a turbulent boundary layer. *AIAA*-87-1309.

ROGALLO, R. S. & MOIN, P. 1984 Numerical simulation of turbulent flows. *Ann. Rev. Fluid Mech.* **16**, 99.

SHABAKA, I. M. M. A., MEHTA, R. D. & BRADSHAW, P. 1985 Longitudinal vortices imbedded in turbulent boundary layers. Part 1. Single vortex. *J. Fluid Mech.* **155**, 37.

TAYLOR, A. M. K. P., WHITELAW, J. H. & YIANNESKIS, M. 1984 Developing flow in S-shaped ducts II. Circular cross-section ducts. *NASA CR* 3759.

WESTPHAL, R. V., EATON, J. K. & PAULEY, W. R. 1987 Interaction between a vortex and a turbulent boundary layer in a streamwise pressure gradient. In *Turbulent Shear Flows 5* (ed. F. Durst *et al.*), p. 266. Springer.

WESTPHAL, R. V. & MEHTA, R. D. 1987 Interaction of an oscillating vortex with a turbulent boundary layer. *AIAA*-87-1246.